RESEARCH ARTICLE

Terra Nova WILEY

Active faulting in the Beagle Channel (Tierra del Fuego)

Donaldo Mauricio Bran[1,2] | Fermín Palma[1,2] | Marco Menichetti[3] | Emanuele Lodolo[4] | Stefania Bunicontro[1,2] | Jorge Gabriel Lozano[1,2] | Luca Baradello[4] | Diego Winocur[1,5] | Maurizio Grossi[4] | Alejandro Alberto Tassone[1,2]

[1]Universidad de Buenos Aires, Facultad de Ciencias Exactas y Naturales, Depto. De Ciencias Geológicas, Buenos Aires, Argentina

[2]CONICET-Universidad de Buenos Aires, Instituto de Geociencias Básicas, Aplicadas y Ambientales de Buenos Aires (IGeBA), Buenos Aires, Argentina

[3]Dipartimento di Scienze Pure ed Applicate–Università di Urbino, Urbino, Italy

[4]Istituto Nazionale di Oceanografia e di Geofisica Sperimentale (OGS), Trieste, Italy

[5]CONICET-Universidad de Buenos Aires, Instituto de Estudios Andinos "Don Pablo Groeber" (IDEAN), Buenos Aires, Argentina

Correspondence
Donaldo Mauricio Bran, Universidad de Buenos Aires, Facultad de Ciencias Exactas y Naturales, Depto. De Ciencias Geológicas. Buenos Aires, Argentina.
Email: dbran@gl.fcen.uba.ar

Abstract

In Tierra del Fuego, the Magallanes-Fagnano Fault System (MFFS) accommodates a significant portion of the relative motion between the South America and Scotia plates. However, it remains unclear whether some of the deformation is partitioned southwards, along the Beagle Channel Fault System (BCFS). In this paper, high-resolution seismic reflection profiles were used to identify fault-related ruptures in the submerged Quaternary sediments of the Beagle Channel. Some faults reach the seafloor, affecting marine sediments, indicating they are Holocene in age. The correlation with outcrop data and lineaments mapped onshore suggests the post-glacial re-activation of two structures: the E-W striking BCFS and the NW-SE-trending Lapataia Fault Zone (LFZ). Whereas the BCFS displays along-strike variation in throw, the LFZ shows significant normal displacements. These results imply that deformation occurs in a wider and more complex manner than previously thought and highlight the need for a thorough hazard assessment of the area.

1 | INTRODUCTION

Identifying active structures in humid, formerly glaciated regions can be difficult because faults usually run underwater or their primary geomorphological markers can be obscured by dense forests, or peatlands. In such cases, subaqueous sediments provide an alternative, highly valuable record to reveal recent tectonic deformation (De Batist et al., 2017; McCalpin, 2009). Subaqueous sediment ruptures have been imaged using high-resolution seismic reflection methods in different tectonic settings (Armijo et al., 2005; Barnes & Pondard, 2010; de La Taille et al., 2015; Doughty et al., 2013; Villalobos et al., 2020) demonstrating that they are a crucial technique for characterizing neotectonics in high-sedimentation, post-glacial environments, as

in the case of lakes and fiords of southern Tierra del Fuego (Bartole et al., 2008; Brambati et al., 1991; Lodolo et al., 2003).

The Fuegian archipelago is traversed by the Magallanes-Fagnano Fault System (MFFS) (Figure 1a), part of the transform boundary between South America and Scotia plates, active since the late Oligocene, linked to the opening of the Drake Passage (Barker, 2001; Dalziel et al., 2013; Lagabrielle et al., 2004; Livermore et al., 2005, 2007; Lodolo et al., 2006; Maldonado et al., 2014; Vérard et al., 2012). The MFFS system is composed of discrete strike-slip fault segments with predominantly sinistral kinematics and an *en-echelon* geometry (Lodolo et al., 2003; Menichetti et al., 2008; Sue & Ghiglione, 2016) and is assumed to accommodate most of the deformation along this segment of the plate boundary (Lodolo et al., 2003; Mendoza et al., 2011; Onorato
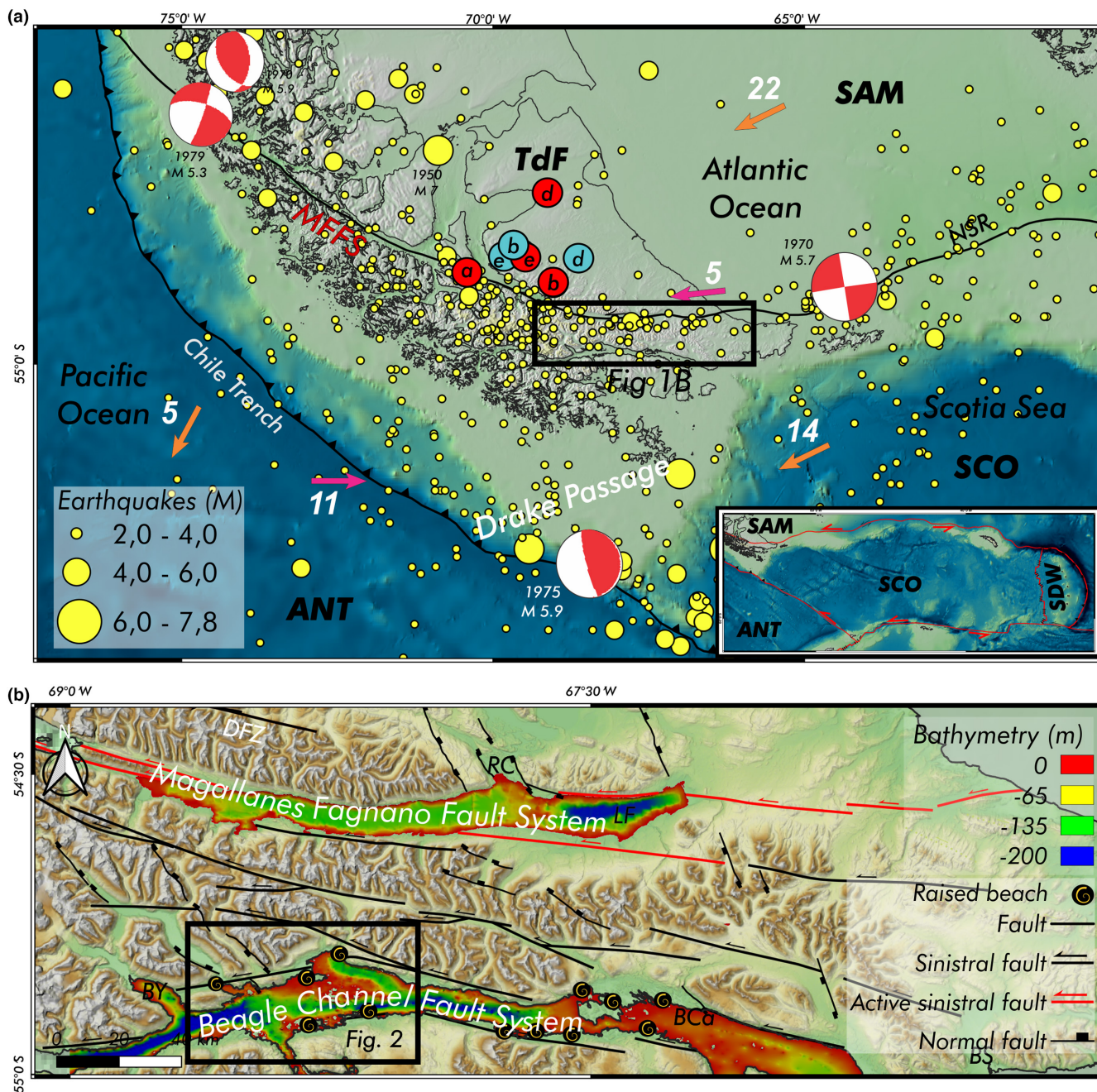
wileyonlinelibrary.com/journal/ter

FIGURE 1 (a) Regional tectonic map of Tierra del Fuego (TdF). ANT, Antarctic Plate; MFFS, Magallanes—Fagnano Fault System; SAM, South American Plate; SCO, Scotia Plate. Seismicity epicentres are from the Seismological Reference Catalogue (Sabbione et al., 2007; Connon et al., 2021), Ml: local magnitude. Focal mechanisms are from Forsyth (1975) and Pelayo and Wiens (1989). The epicentres for the 1949 earthquakes are adapted from Roy et al., 2020, with the Mw 7.75 in red and the Mw 7.5 in pale blue, according to: (a) Castano (1977), (b) Jaschek et al. (1982), (c) Pelayo and Wiens (1989) and (d) Bondár et al. (2015). The red orange and pink arrows indicate absolute (relative to the hotspot reference frame of Minster & Jordan, 1978) and relative (to the Scotia Plate) (Pelayo & Wiens, 1989) plate motion values in mm/yr, respectively. Bathymetric data is from GECBO (https://www.gebco.net/data_and_products/gridded_bathymetry_data/). The inset map shows the present-day geodynamic scenario. (b) Map of the southern part of Tierra del Fuego with the main transcurrent structures. There are two main fault systems: the MFFS in the north, with several fault segments that were active after deglaciation, and the BCFS in the south. Note that the main E-W morphostructural elements are interspersed with a series of NW-SE striking lineaments. Modified from Menichetti et al. (2008) and Roy et al. (2020). Elevated marine deposits along the shores of the BC are from Björck et al. (2021), Bujalesky (2007), Gordillo et al. (1992), McCulloch et al. (2019) . The Digital Elevation Surface (DSM) is the Alos World 3D model from JAXA (https://www.eorc.jaxa.jp/ALOS/en/dataset/aw3d_e.htm. Bathymetry of Lago Fagnano and Beagle Channel are from Zanolla et al. (2011) and Esteban et al. (2013) respectively. EQ, Earthquakes; RC, Rio Claro; LF, Lago Fagnano; BY, Bahía Yendegaia; BCa, Bahía Cambaceres; BS, Bahía Sloggett; DFZ, Deseado Fault Zone.
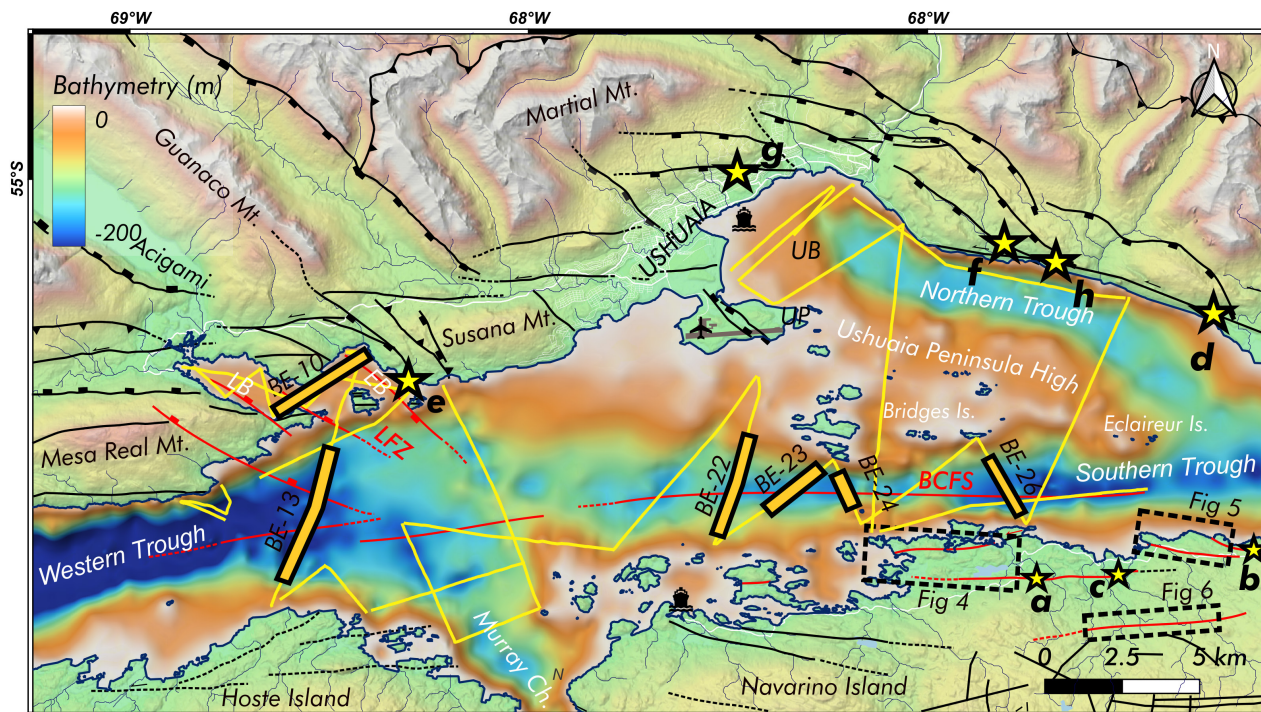
FIGURE 2 Structural and bathymetric map of the central Beagle Channel. Yellow lines show the location of the high-resolution seismic profiles. The seismic sections presented in this work are indicated by thick yellow segments. The references are as in Figure 1. The red lines depict active faults segments reported in this work. BCFS, Beagle Channel Fault System; LFZ, Lapataia Fault Zone; BL, Bahía Lapataia; BE, Bahía Ensenada; PU, Peninsula Ushuaia. Bathymetry data was modified from Esteban et al. (2013).
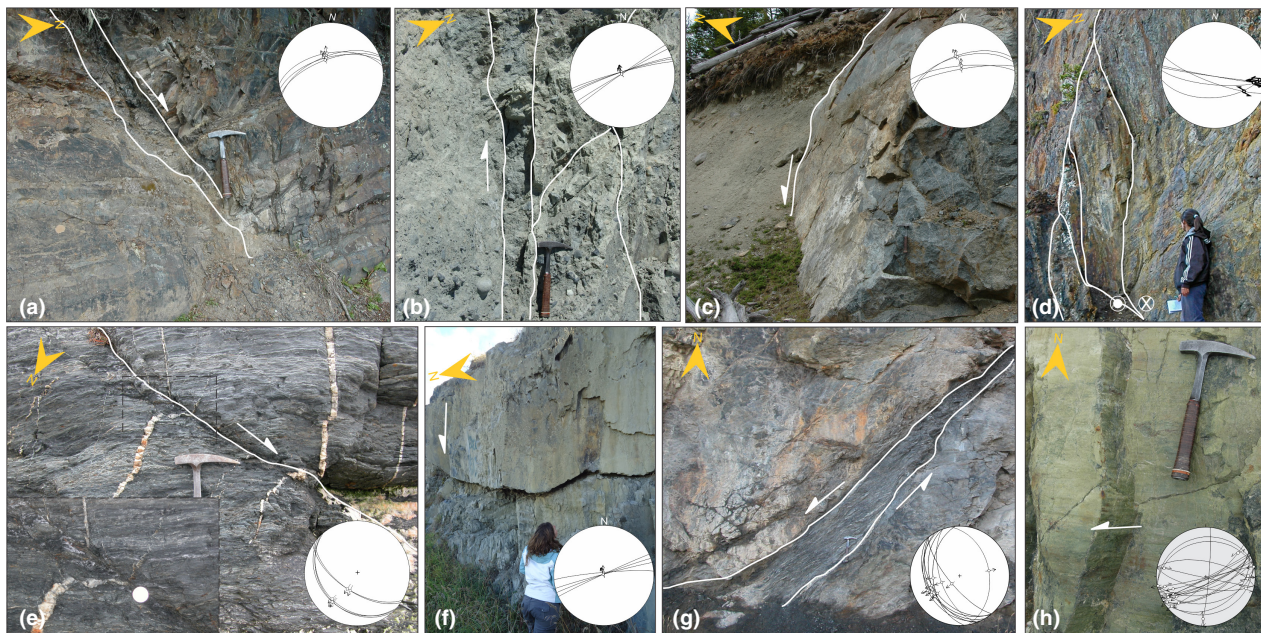

FIGURE 3 Photographs of the outcrop sites with the main structural and geometrical characteristics of the faults associated to transcurrent deformation along the BCFS. Fault planes great circles and related striae (arrows) are projected in the lower hemisphere equal-area plots for each outcrop. The site positions are indicated in Figure 2 as yellow stars with lowercases. (a) Northwards-dipping normal fault on Upper Cretaceous rocks of Yahgan Fm. in Navarino Island. (b) Vertical fault plane with fault gauge on glacial sediments located to the east of A. (c) Outcropping normal fault plane forming a scarp in Navarino Island. (d) Left lateral strike-slip fault planes affecting cretaceous rocks of Yaghan Fm along the northern BC coast. (e) Southwest-dipping low-angle normal fault affecting phyllites of Lapataia Fm. Displacement on tension quartz veins are of several centimetres. (f) Vertical normal fault plane on rocks of Yahgán Fm outcropping in Ushuaia city. (g) Southwest-dipping extensional shear zone on slaty Yahgan Fm, striking parallel to the coastline of the northern trough. (h) Left-lateral mesoscale strike-slip fault developed on rocks of Yahgan Fm.
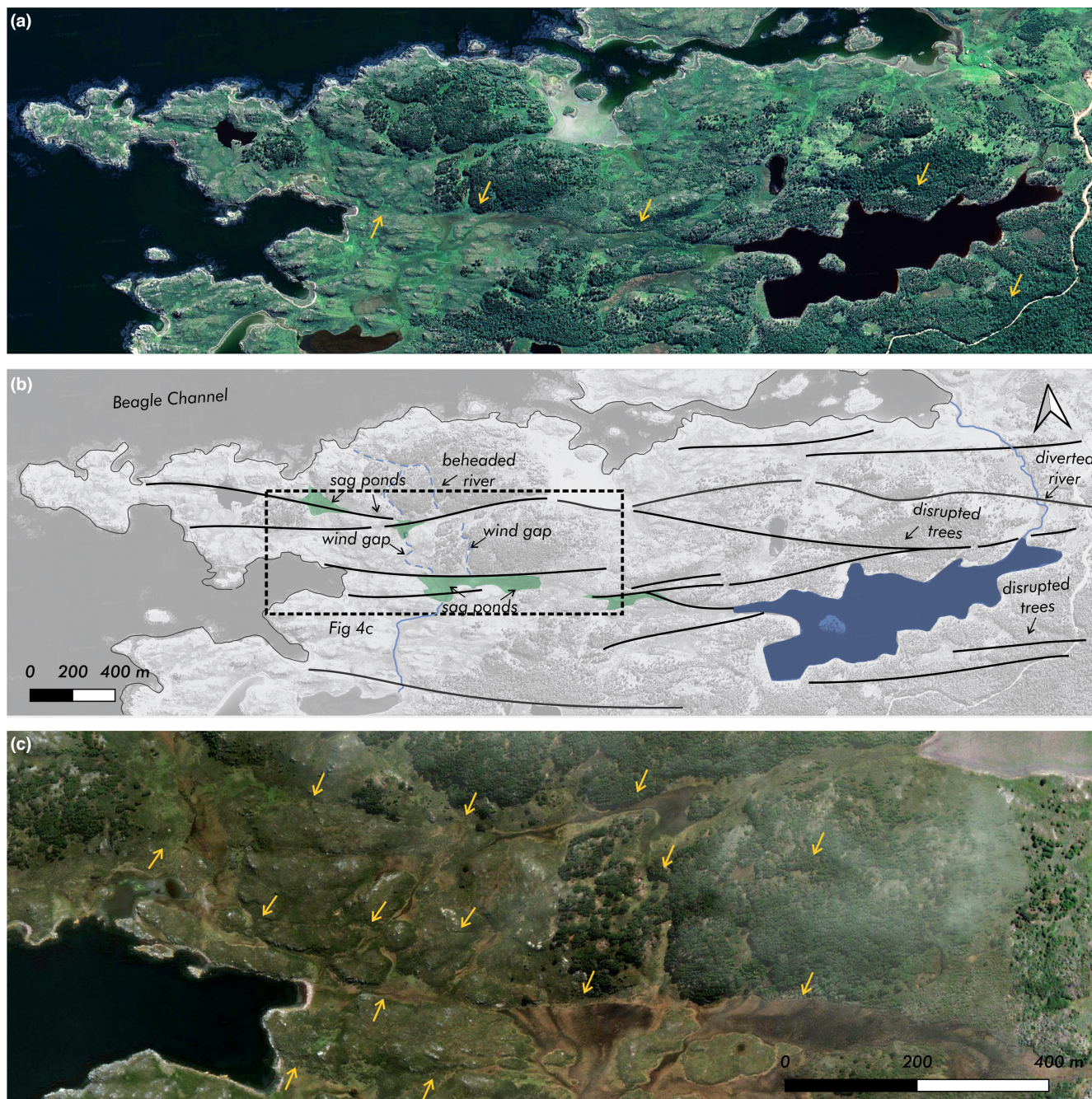
FIGURE 4 Google Earth image showing geomorphological markers that may suggest active deformation along the northern sector of Navarino Island. Lineaments associated to sag ponds and drainage anomalies such as channel divertions, beheaded rivers and linear streams can be observed. The yellow arrows in (a) indicate the features mapped in the line drawing (b). Figure (c) is a close-up of the lineaments. The location of the image is indicated in Figure 2.

et al., 2021; Roy et al., 2020; Sandoval & De Pascale, 2020). However, uncertainty remains about whether and where part of deformation is distributed off the MFFS (Klepeis, 1994; Sandoval & De Pascale, 2020).

The area has experienced large historical earthquakes with estimated magnitudes higher than 7 (Figure 1a) (Cisternas & Vera, 2008; Pelayo & Wiens, 1989). Meanwhile, the background seismicity is dominated by shallow low-magnitude events (M < 3.5), distributed along the MFFS and to the south of its trace (Ammirati et al., 2020; Buffoni et al., 2009; Febrer et al., 2000).

The regional-scale Beagle Channel Fault System (BCFS), to the south of the MFFS, is a major crustal structure. It has had a major role controlling deformation at least since the Late Cretaceous, during the closure and inversion of Rocas Verdes marginal basin and the Andean orogenesis (Cunningham, 1995; Dalziel & Brown, 1989; Klepeis et al., 2010; Nelson et al., 1980). During the Cenozoic, a transcurrent system, with predominantly strike-slip and normal faults that cross-cut Andean structures, developed along the BCFS (Cunningham, 1993, 1995; Klepeis et al., 2010; Menichetti
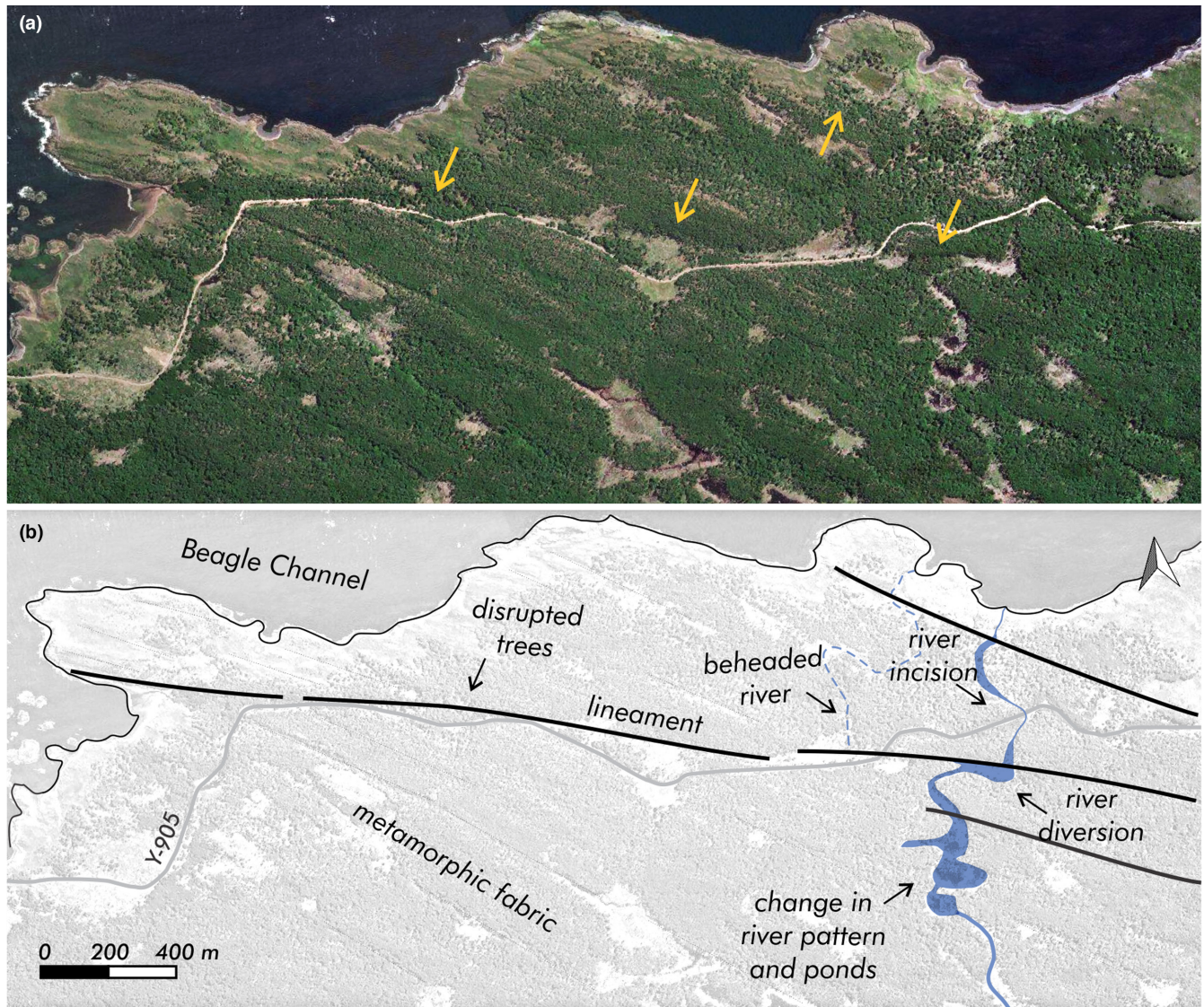
FIGURE 5 a) Google Earth image of northern Navarino Island. b) Interpretation line-drawing. To the north of the road is a conspicuous lineament, in the form of a linear scarp and aligned forest. A stream draining from the south begins to wonder as it approaches the lineament, until it manages to cut through it. The lineament obliquely traverses the NW-SE striking folded and foliated fabric of the metasedimentary rocks of the Yahgan Fm. Yellow arrows indicate the lineament trace in the image. The location of the image is indicated in Figure 2.

et al., 2008). Neotectonic activity along this system is suspected (Bran et al., 2017; Bujalesky, 2011; Gordillo et al., 1992; Mörner, 1991), but no conclusive evidence has yet been presented.

Therefore, we conducted a high-resolution seismic reflection survey along the central sector of the Beagle Channel to verify the presence of deformation in the Quaternary sediments of the basin and to evaluate the role of the BCFS in the regional structural framework of the plate boundary.

2 | METHODOLOGY

The seismic reflection survey was carried out in the Beagle Channel using a Boomer system, shooting 150 J every 0.5 s and a single-channel,

high-sensitivity 10-hydrophone solid-state streamer (bandwidth of 100–10.000 Hz). The sampling rate was 0.05 ms and the recording length 400 ms. Data have been acquired with a ship speed of about 4 knots and were processed using Paradigm Echos software and Seismic Unix. It included gain and time-variant filtering, and spiking deconvolution. Seismic lines were interpreted using IHS Markit Kingdom® software.

Field data on outcrops were collected during a series of field campaigns. Structural analyses and equal-area plots were produced using Win-Tensor software (Delvaux & Sperner, 2003). The open-source software QGIS was used for geomorphological mapping and processing of bathymetric and digital elevation data grids (QGIS Geographic Information System. Open-Source Geospatial Foundation Project; http://qgis.osgeo.org).
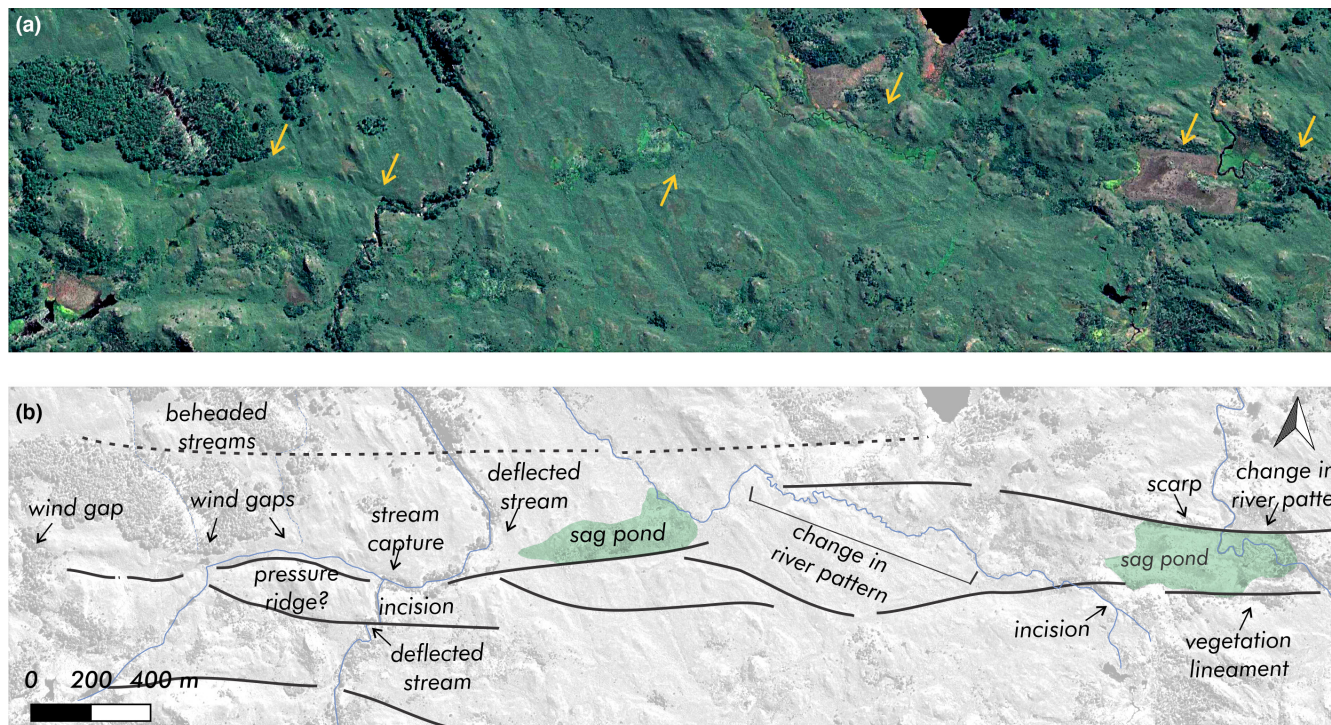
FIGURE 6 a) Google Earth image of northern Navarino Island. b) Interpretation line-drawing. A E-W irregular lineament cuts through the regional NW-SE foliated pattern. Several sag ponds can be observed, associated with changes in the river pattern. A river capture has produced the abandonment of some channels to the west, giving as a result several wind gaps and beheaded channels. Yellow arrows indicate the lineament trace in the image. The location of the image is indicated in Figure 2.

3 | MORPHOSTRUCTURE OF THE CENTRAL BEAGLE CHANNEL

The Mesozoic metavolcanic and metasedimentary rocks in the Beagle Channel's central segment are affected by two fault systems (Bran et al., 2017; Menichetti et al., 2008; Peroni et al., 2009): (1) a W-E to WSW-ENE striking sub-vertical transcurrent system (BCFS), and (2) transverse NW-SE striking predominantly extensional fault system with gentler dipping fault planes, such as the Lapataia Fault Zone (LPZ) (Figures 2 and 3). Cross-cutting relationships indicate that all these faults post-date the Andean contraction (Klepeis et al., 2010; Menichetti et al., 2008). These fault systems have visibly influenced the submerged morphology of the BC. The E-W southern trough features an irregular seafloor with several rhombic-shaped sub-basins, while the oblique bays, parallel to the transverse normal fault system, are flat-floored with symmetrical transverse section (Figure 2).

Due to the absence of well-preserved Quaternary deposits, it is difficult to assess the activity of the structures affecting the central BC. A glacial deposit exposed in a road cut with a one-meter-wide E-W striking sub-vertical fault zone and top-down-to-the-north normal movement (Figure 3b) suggests the possibility of Quaternary fault activity. In addition, a series of lineaments (Figures 4, 5 and 6) comprises further evidence of neotectonics along the BCFS. The geomorphological markers include sag ponds, diverted streams or changes in the river pattern, wind gaps, disrupted or aligned forests. To accurately
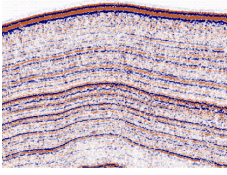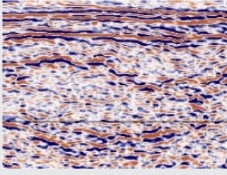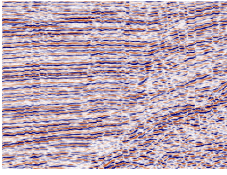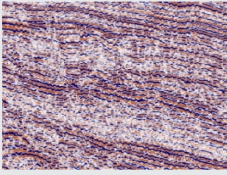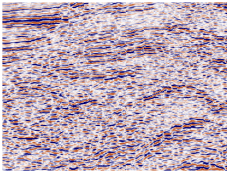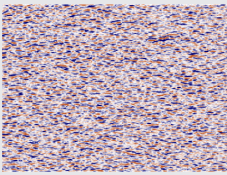
evaluate the significance of these evidences in terms of modern deformation, a detailed examination of the submerged sedimentary record of the BC is necessary

4 | DEFORMATION IN THE BEAGLE CHANNEL SEDIMENTS

4.1 | Beagle Channel's seismic stratigraphy

For the general seismic stratigraphy of the Beagle Channel, we follow the works of Bujalesky, Aliotta, and Isla (2004) and Bran (2019). Both works recognize an acoustically chaotic to semi-transparent till and related glaciogenic sediments as the oldest deposit resting over an acoustically transparent bedrock, constituted by Mesozoic rocks (Table 1). Overlying the till or the bedrock there is a layered unit with sub-parallel laterally onlapping reflections interpreted as glaciolacustrine sediments (Bujalesky, Aliotta & Isla, 2004, Bujalesky, Coronato & Roig, 2004), which were dated as ca. 16 cal kas BP from an onshore core in the northern shore of Isla Navarino (Björck et al., 2021; McCulloch et al., 2019; McCulloch et al., 2020). Glaciofluvial units are locally recognized in Golondrina, Ushuaia and Lapataia bays (Bran, 2019; Bujalesky, Aliotta & Isla, 2004; Bujalesky, Coronato & Roig, 2004; Bujalesky, 2007). These comprise prograding deltaic facies with paleochannels and reflections of low amplitude corresponding to submerged alluvial plains (Table 1). The uppermost draping unit,

TABLE 1 General seismic stratigraphy of Beagle Channel's sedimentary infill

Unit	Acoustic properties	Example
Marine	Parallel reflections. High frequency and low to medium amplitude. Draping geometry.	
Glaciofluvial	Low-amplitude discontinuous reflections. Erosive truncations. Lens-shaped geometries. Palaeochannels	
Glaciolacustrine	Onlapping high-amplitude, sub-parallel, continuous reflections. Upwards increase in frequency	
MTD	Lens-shaped, acoustically chaotic, irregular top	
Till	Wavy discontinuous reflections. Hummocky or chaotic. Ridge-like morphologies	
Bedrock	Acoustically transparent	

consisting of high-frequency parallel reflections of medium amplitude, corresponds to marine sediments deposited after the early-Holocene transgression, dated as ca. 8.5 cal kas BP from onshore cores (Candel et al., 2018; McCulloch et al., 2019). In some places, there are lens-shaped acoustically chaotic bodies interlayered within the stratified infill, interpreted as Mass Transport Deposits (MTDs).

4.2 | Southern trough

In the Southern Trough, the area between Ushuaia Peninsula and Navarino Island displays significant sediment deformation. From east to west, the line BE-26 shows well-layered onlapping reflections that are laterally truncated and displaced by sub-vertical (>60°) fault ruptures, with offsets not exceeding ~3 m (Figure 7). The faults affect the

glaciolacustrine seismic unit and can be traced into the glacial unit. The reflections are slightly folded or tilted towards the fault planes.

Westwards, seismic line BE-24 shows a symmetrical profile with steep lateral margins and an onlapping fill consisting of parallel high-amplitude reflections (Figure 8). Sediment deformation is evidenced as lateral truncations, diffractions and tilted and folded reflections. The discontinuities that obliterate the layered reflections, interpreted as glaciolacustrine seismic unit, are sub-vertical (>60°) and are mainly located in the southern half of the trough (Figure 8).

Line BE-23 shows a vertical deformation zone that crosscuts the parallel horizontal reflections (Figure 9). There are several lens-shaped MTDs interlayered within both glaciolacustrine and marine units. The geometry of the deposits suggests that they originated from slope failures in the southern flank of the channel.

On the BE-22 deformation concentrates along the southern margin of the trough. In this area, reflections are truncated and folded by a series of vertical discontinuities (Figure 10) forming a ~1 km wide deformation zone that involves both glaciolacustrine and marine seismic units. The northern part of the line shows undeformed sediments.

4.3 | Western trough

Line BE-13 shows that the reflections corresponding to the uppermost draping marine unit are obliterated by sub-vertical discontinuities (Figure 11). While some of the discontinuities reach the seafloor, others terminate at ~0.025 s below this surface. In the northern part, as the line approaches the LFZ, wedge-shaped seismic facies and reflections onlap against a sub-vertical to NE-dipping faults (Figure 11), involving some meter-scale normal offsets, that affect up to the seafloor and produce bathymetric steps.

Seismic line BE-10, located to the northeast, displays a series of graben-like sub-basins (Figure 12), filled with glaciolacustrine, glaciofluvial and marine sediments. The reflections in this area are also vertically displaced by faults, with normal offset values that reach up to ~6 m. In this case, the ruptures affect glaciolacustrine and glaciofluvial units but seem to be truncated by the marine transgression unconformity (Figure 12).

5 | DISCUSSION

Neoteconic markers documented along the MFFS (Onorato et al., 2021; Roy et al., 2020; Sandoval & De Pascale, 2020) yielded ages ranging from 18 to 26 ka (Onorato et al., 2020; Roy et al., 2020), indicating that Quaternary deformation began to manifest in the Fuegian landscape during and after glacier recession. To the north, kinematic analyses and some morphological evidence (Klepeis, 1994; Sandoval & De Pascale, 2020) suggest that the Deseado Fault accommodated sinistral strike-slip motion during the Quaternary. Our analysis indicates that the BCFS also experienced deformation pulses following glacial recession, implying a wider
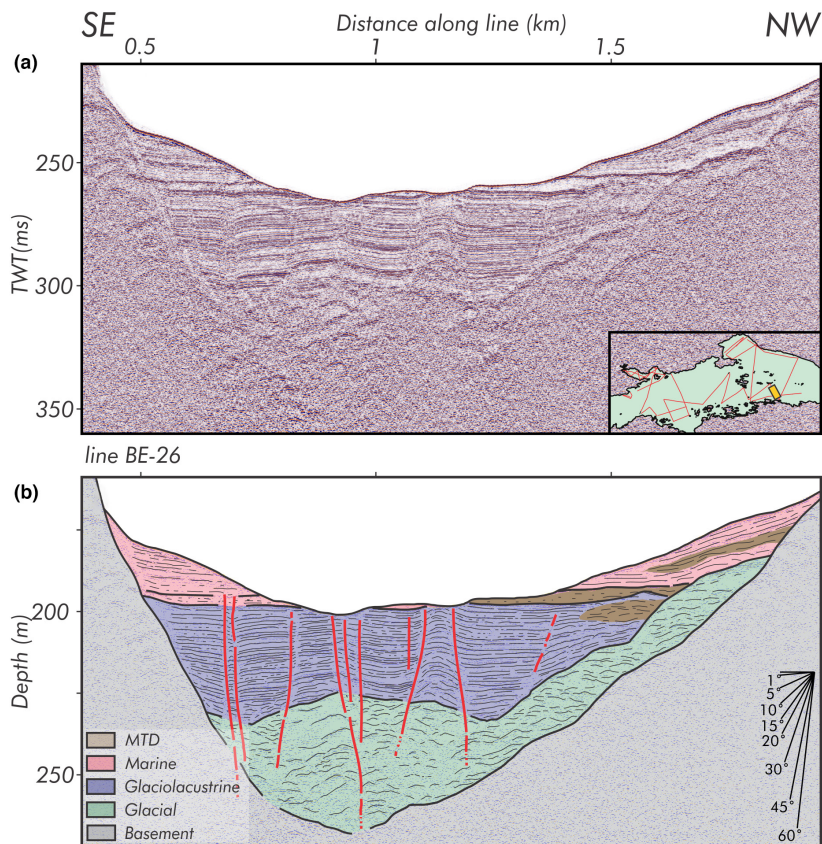
FIGURE 7 (a) Seismic line BE-26. The inset map shows the location of the line. (b) Line drawing and interpretation. Note the layered reflections (sedimentary strata) that are cut by a series of sub-vertical faults. The trough has a southern margin steeper than the northern one. Some tilting and minor dowthrowing can be recognized within the reflections, resembling a negative flower structure. The seafloor erosional unconformity has removed most of the marine deposits from central part of the trough, although they can be recognized towards the flanks. Vectors in the bottom left corner show angular relationships.
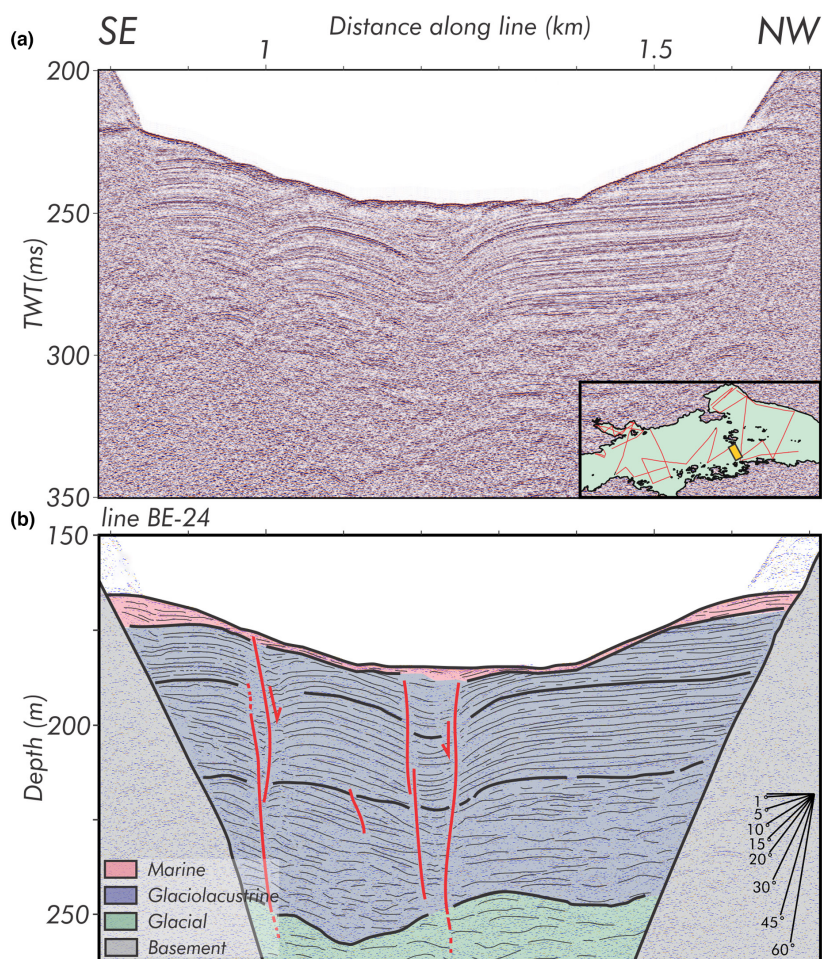

FIGURE 8 (a) Seismic line BE-24. In this area the trough has a symmetrical cross-section with a laterally onlapping basin fill. Note the reflections that curve towards a series of sub-vertical discontinuities. The inset map shows the location of the line. (b) Line drawing and interpretation. Deformation nucleates in the southern half of the line. In this area reflections are tilted towards the basin centre. Vectors in the bottom left corner show angular relationships.

FIGURE 9 (a) Seismic line BE-23. (b) Interpretation line drawing with a sub-vertical deformation zone that affect the well-stratified glaciolacustrine and marine sediments. A series of lens-shaped acoustically chaotic bodies can be recognized in the southern part of the seismic line, corresponding to mass transport deposits. The downlap terminations and the thinning towards the north indicate that the deposits were originated from slope failures at the southern margin of the trough. The number of MTDs found in this section suggest that they constitute recurrent events.
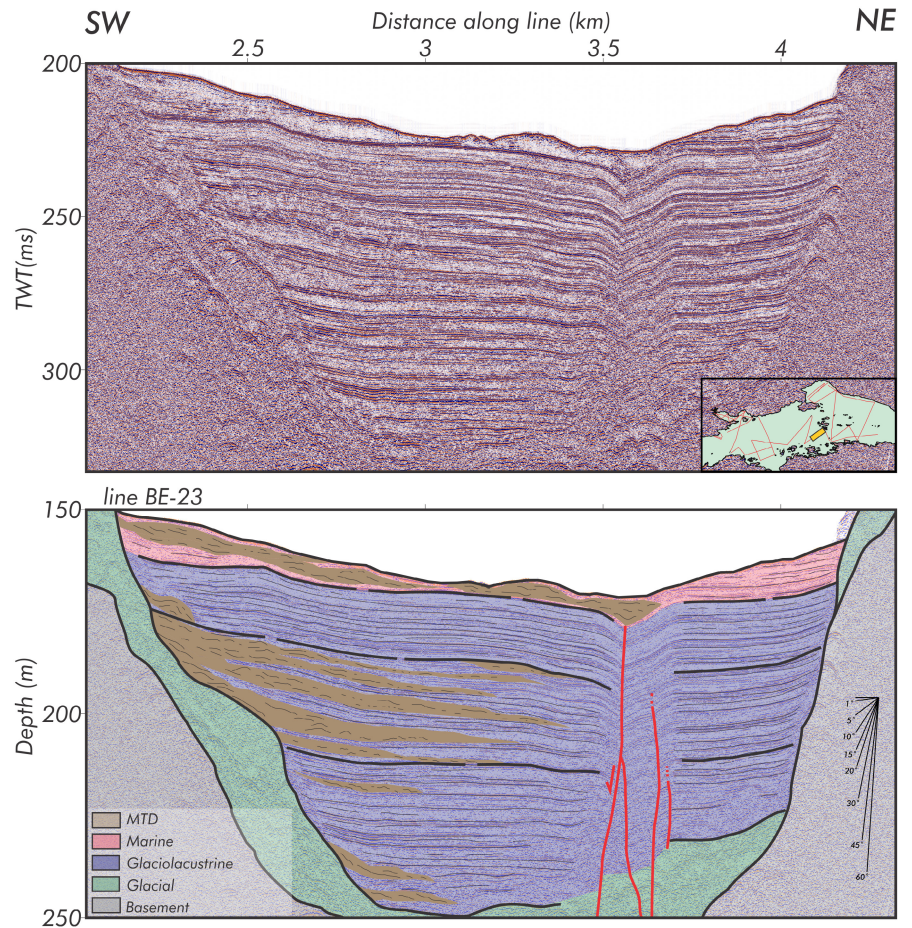

FIGURE 10 (a) Detail of seismic line BE-22. The trough shows a fairly symmetric profile with an onlapping fill constituted by parallel high amplitude reflections that become obliterated in the south by a series of discontinuities. The inset map shows the location of the line. (b) Interpretation line drawing with a series of steeply dipping fault ruptures affecting the sediments clustered in the southern part of the trough. Reflections are folded in association with the fault planes, with a positive flower shape. Vectors in the bottom left corner show angular relationships.
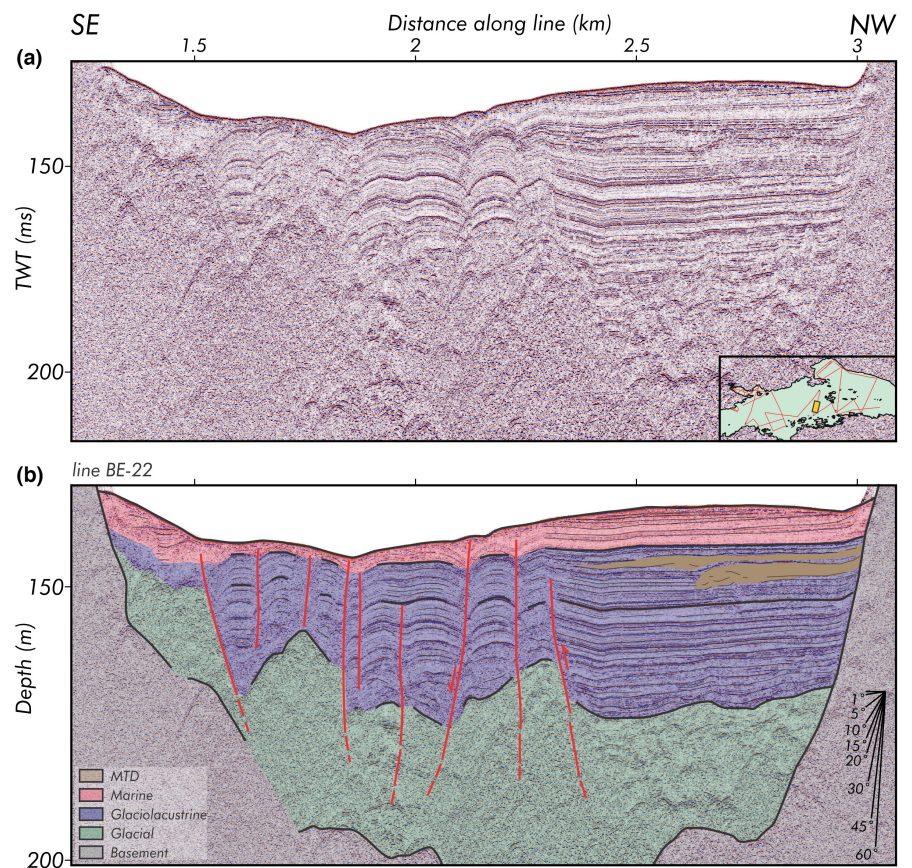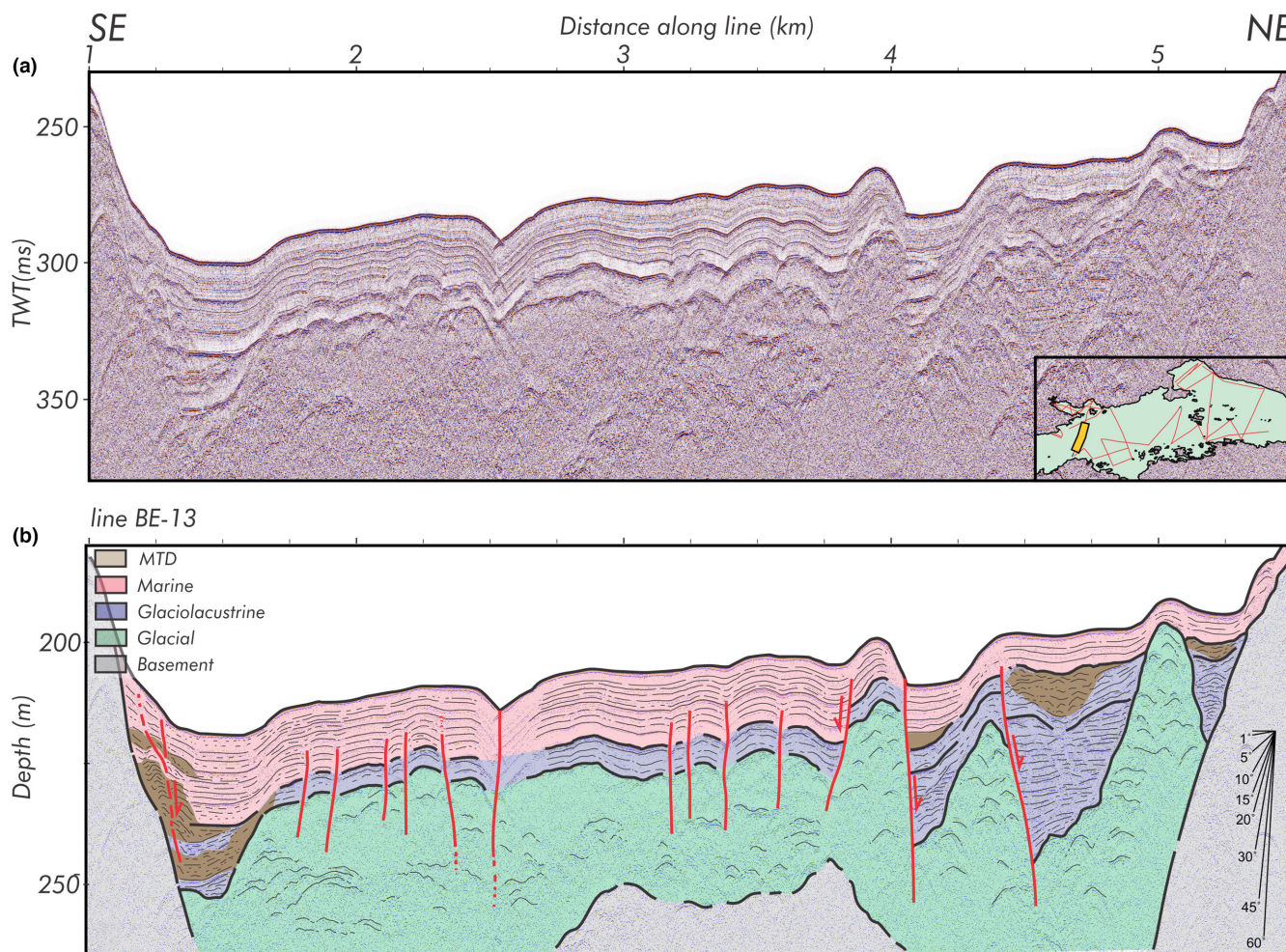
FIGURE 11 (a) Seismic line BE-13. Here the trough is wider than in the eastern lines and shows a symmetrical profile with an irregular seafloor. The inset map shows the location of the line. (b) Line drawing and interpretation of profile BE-13. The thicker marine unit shown in this profile with respect to the previous seismic lines is due to its proximity to Yendegaia bay. At the head of the bay, sedimentary plumes from the Yendegaia river delta extend to the BC. In the south-central part of the line the reflections are truncated by vertical discontinuities. The most prominent discontinuity affects all units and causes a pull-down of the seafloor. However, the vertical discontinuities on each side of the later do not reach the seafloor. The northern zone is characterized by a staircase shape of the seafloor associated with fault that laterally juxtapose different seismic facies, with notable normal offsets. Note that glaciolacustrine deposit filling small sub-basin show divergent seismic reflections, thickening towards the rupture planes.

(~75 km) deformation zone for the plate boundary than it was previously assumed (i.e. 30 to 50 km; Mendoza et al., 2015; Sandoval & De Pascale, 2020). The less clear morphological expression to the south of the MFFS, however, could be explained by a slower deformation rate and/or by the fact that most of the tectonic activity is actually expressed along the submerged part of the BC.

It must be emphasized, however, that in many examples of transform systems along plate boundaries, relative motion between plates does not occur exclusively along a single, master fault, but is distributed over a more or less large deformation zone comprising several faults running sub-parallel to the main fault, as documented in other strike-slip tectonic environments similar to those of the South America-Scotia plate boundary (e.g. Lodolo et al., 2009; Obrist-Farner et al., 2020).

Assuming that the central sector of the Beagle Channel was ice-free at ca. 17 cal ka BP (Hall et al., 2013; McCulloch et al., 2020),

faulted glacial and glaciolacustrine deposits imply that the BCFS underwent deformation pulses during the latest Pleistocene. There is yet no dating from sediment offshore cores within central BC, but some of the faults affect marine deposits and rupture to the seafloor (e.g. Figures 7 and 11) indicating that some of the pulses occurred as early as the Holocene, postdating the ca. 8.5 cal ka BP transgression (Candel et al., 2018; McCulloch et al., 2019; Rabassa et al., 1986).

The fault ruptures found along the Southern Trough can be traced, from the available seismic data, from the Eclaireurs to the Hoste Islands (Figure 2b). These are part of an active E-W fault strand of the BCFS (Figure 2), that extends largely underwater but may be linked to the onshore lineaments mapped in northern Navarino Island (Figures 4, 5 and 6). The seismic profiles across the BCFS show sub-vertical flower structure and variable vertical slip component, with local transpressional (Figure 10) or transtensional (Figures 7 and 8) zones. This along-strike variation in deformation style also characterizes the MFFS to
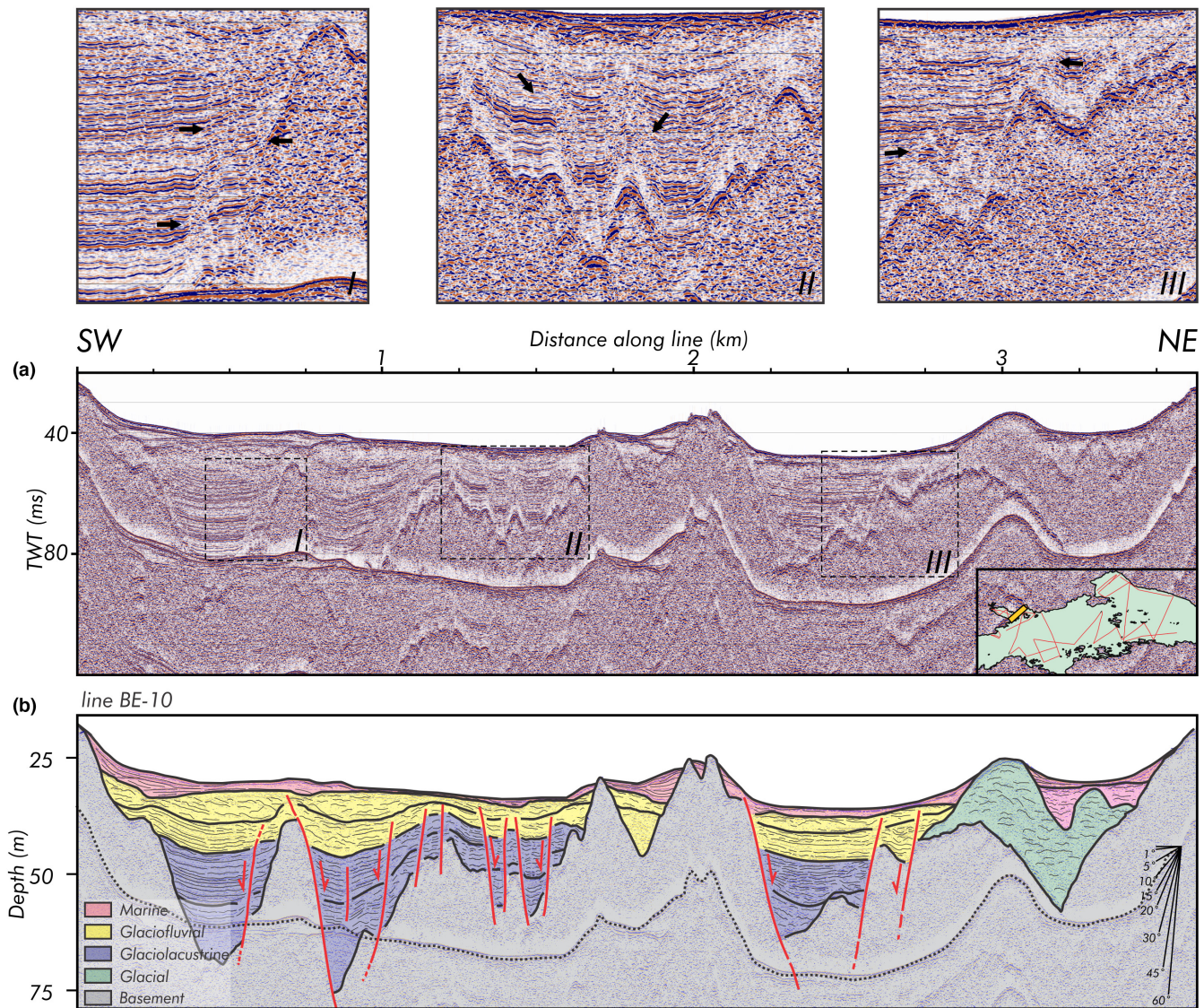
FIGURE 12 (a) SW–NE oriented seismic line be-10 at Lapataia and Ensenada Bays. (b) Line drawing and interpretation of profile BE-10 reveals two fault-bounded basins controlled by the LPZ. The Lapataia Bay consist of two sub-basins separated by a bedrock high. In both basins, a system of normal faults cross-cut the modern sedimentary infill. Reflections in the deeper glaciolacustrine unite show vertical displacements of up to 6 m, whereas those in the younger glaciofluvial unit have almost 2 m of displacement. The decreasing magnitude of the displacements from bottom to top suggests that multiple deformation events may have caused a cumulative slip.

the north (Onorato et al., 2020; Roy et al., 2020), indicating a structural consistency between both fault systems in terms of how they accommodate deformation.

On the other hand, the ruptures found at the LFZ are related to transverse faults and show graben-like structures with significant normal offsets affecting post-glacial glaciolacustrine deposits (Figures 11 and 12). Extensional deformation along transverse NW-SE striking structures has already been recognized in several parts of southern Tierra del Fuego (Bran et al., 2017; Ghiglione et al., 2008; Klepeis, 1994, 2010; Lodolo et al., 2003; Menichetti et al., 2008), cutting through Andean contractional structures. Neotectonic activity has been suggested for these faults at least in the Rio Claro graben and in the Sloggett Bay (Figure 1b; Lodolo

et al., 2003; Rabassa et al., 2004), located in the easternmost BC (Figure 1b), where late Holocene standing tree trunks were found below present-day high tide level (Rabassa et al., 2004). We suggest that these basins are active graben-like structures as those imaged in the LFZ (Figures 11 and 12). Although it is not yet understood how the rupture transfers from strike-slip to normal dip-slip in areas that are obliquely oriented to the main margin trend, this fault geometry may be strongly influenced by the presence of pre-existence structural weaknesses (Bran et al., 2017).

To date, the idea of neotectonic activity within the BC has been largely based on the recognition of elevated marine deposits along the BC coast (Figure 1b) (Bujalesky, Coronato & Roig, 2004; Gordillo et al., 1992; Rabassa et al., 2000). These deposits were interpreted as

the result of regional tectonic uplift (Bujalesky, Coronato & Roig, 2004; Gordillo et al., 1992; Mörner, 1991; Rabassa et al., 2000). However, recent work based on cores and numerical modelling suggests glacio-isostatic rebound as the main contributor for the elevated deposits (Björck et al., 2021). Our seismic reflection data results do not show evidence supporting regional tectonic uplift along the BCFS. On the other hand, local tectonic subsidence along LFZ could explain differences in relative elevation within terraces mentioned within the bays (Björck et al., 2021; Borromei & Quattrocchio, 2007; Mörner, 1991).

Finally, the identification of widespread subaerial and subaqueous MTDs nearby active faults in the BC region (this work, Bran et al. (2020), Bran et al. (n.d.)) suggest a potential link of slope failure with seismic activity. In this sense, the stacked deposits in Figure 9 imply a recurrence of slope failures events, as was observed by Waldmann et al. (2011) in Lago Fagnano to the north. The likely connection between MTDs and earthquakes provides an opportunity to investigate and refine the paleoseismicity of the area. Furthermore, it warrants an evaluation of the geological hazards associated with these events.

6 | CONCLUSIONS

Even though deformation in this segment of the South America-Scotia transform boundary is mainly partitioned along faults within the MFFS, some strain is also accommodated to the south along the BCFS. Based on a set of high-resolution seismic profiles, we have documented late Pleistocene to Holocene tectonic activity on the BCFS, extending further south the influence of the plate boundary. The consistency in style and spatial distribution of the modern ruptures within the structural framework of the area suggest they reactivate pre-existing basement structures.

The E-W striking BCFS is characterized by flower-like structures with local transpressive and transtensive deformation in the post-glacial sediments of the Beagle Channel. Ruptures concentrate along the southern margin of the channel and could be linked with lineaments identified on the northern shore of Navarino Island.

The NW-SE striking LFZ shows faults that rupture to the seafloor, with graben-like geometry and significant normal displacements. These structures control the oblique bays on the northern margin of the channel.

Besides the influence of Quaternary tectonics on the Fuegian landscape, this work also emphasizes the importance of conducting a comprehensive assessment in the area, not only to map active fault segments but also to investigate the occurrence of associated geohazards such as landslides and tsunami.

CONFLICT OF INTEREST STATEMENT
None.

DATA AVAILABILITY STATEMENT
The data that support the findings of this study are available from the corresponding author upon reasonable request.

REFERENCES
Ammirati, J.-B., Flores, M. C., & Ruiz, S. (2020). Seismicity along the Magallanes-Fagnano fault system. *Journal of South American Earth Sciences*, *103*, 102799.

Armijo, R., Pondard, N., Meyer, B., Uçarkus, G., de Lépinay, B. M., Malavieille, J., Dominguez, S., Gustcher, M. A., Schmidt, S., Beck, C., Çagatay, N., Çakir, Z., Imren, C., Eris, K., Natalin, B., Özalaybey, S., Tolun, L., Lefèvre, I., Seeber, L., ... Sarikavak, K. (2005). Submarine fault scarps in the Sea of Marmara pull-apart (North Anatolian Fault): Implications for seismic hazard in Istanbul. *Geochemistry, Geophysics, Geosystems*, *6*(6), Q06009.

Barker, P. F. (2001). Scotia Sea regional tectonic evolution: Implications for mantle flow and palaeocirculation. *Earth-Science Reviews*, *55*, 1–39.

Barnes, P. M., & Pondard, N. (2010). Derivation of direct on-fault submarine paleoearthquake records from high-resolution seismic reflection profiles: Wairau Fault, New Zealand. *Geochemistry, Geophysics, Geosystems*, *11*(11), Q11013.

Bartole, R., De Muro, S., Morelli, D., & Tosoratti, F. (2008). Glacigenic features and tertiary stratigraphy of the Magellan strait (southern Chile). *Geologica Acta*, *6*(1), 85–100.

Björck, S., Lambeck, K., Möller, P., Waldmann, N., Bennike, O., Jiang, H., Li, D., Sandgren, P., Nielsen, A. B., & Porter, C. T. (2021). Relative sea level changes and glacio-isostatic modelling in the Beagle Channel, Tierra del Fuego, Chile: Glacial and tectonic implications. *Quaternary Science Reviews*, *251*, 106657.

Bondár, I., Engdahl, E. R., Villaseñor, A., Harris, J., & Storchak, D. (2015). ISC-GEM: Global instrumental earthquake catalogue (1900–2009), II. Location and seismicity patterns. *Physics of the Earth and Planetary Interiors*, *239*, 2–13.

Borromei, A. M., & Quattrocchio, M. (2007). Holocene sea-level change inferred from palynological data in the Beagle Channel, southern Tierra del Fuego, Argentina. *Ameghiniana*, *44*, 161–171.

Brambati, A., Fontolan, G., & Simeoni, U. (1991). Recent sediments and sedimentological processes in the Strait of Magellan. *Bollettino di Oceanologia Teorica ed Applicata*, *9*, 217–259.

Bran, D. M. (2019). *Estudio geológico y geofísico del sistema lacustre costero Acigami–Lapataia* (PhD Thesis). Universidad de Buenos Aires.

Bran, D. M., Lozano, J. G., Winocur, D., Menichetti, M., Onnis, L., Lodolo, E., & Tassone, A. A. (2020). The Cerro Guanaco mass movements: A geophysical and morphometric approach on a megalandslide in the Fuegian Andes (Southern Patagonia). *Journal of South American Earth Sciences*, *101*, 102617.

Bran, D. M., Palma, F., Principi, S., Lodolo, E., Baradello, L., Lozano, J. G., & Tassone, A. A. (n.d.). High-resolution seismic characterization of postglacial subaqueous mass movements in the Beagle Channel (Tierra del Fuego, Argentina): Dynamics and tsunami hazard implications. *Natural Hazards*.

Bran, D. M., Tassone, A. A., Menichetti, M., Cerredo, M. E., Lozano, J. G., Lodolo, E., & Vilas, J. F. (2017). Shallow architecture of Fuegian Andes lineaments based on electrical resistivity tomography (ERT). Evidences of transverse extensional faulting in the Central Beagle Channel area. *Andean Geology*, *45*, 1–34.

Buffoni, C., Sabbione, N. C., Connon, G., & Ormaechea, J. L. (2009). Localización de hipocentros y determinación de su magnitud en Tierra del Fuego y zonas aledañas. *Geoacta*, *34*, 75–86.

Bujalesky, G., Aliotta, S., & Isla, F. (2004). Facies del subfondo del canal Beagle, Tierra del Fuego. *Revista de la Asociación Geológica Argentina*, *59*, 29–37.

Bujalesky, G., Coronato, A. M. J., & Roig, C. (2004). Holocene differential tectonic movements along the argentine sector of the Beagle Channel (Tierra del Fuego) inferred from marine paleoenvironments. In *GEOSUR 2004, In: International symposium on the geology and geophysics southernmost Andes*. Aires.

Bujalesky, G. G. (2007). Coastal geomorphology and evolution of Tierra del Fuego (southern Argentina). *Geologica Acta*, *5*(4), 337–362.

Bujalesky, G. G. (2011). *The flood of the Beagle Valley (11.000 YR BP), Tierra del Fuego* (pp. 5–21). Anales Del Instituto de La Patagonia.

Candel, M. S., Borromei, A. M., & Louwye, S. (2018). Early to middle Holocene palaeoenvironmental reconstruction of the Beagle Channel (southernmost Argentina) based on terrestrial and marine palynomorphs. *Boreas*, *47*, 1072–1083.

Castano, J. C. (1977). Zonificación sísmica de la República Argentina. Instituto Nacional de Prevención Sísmica. *Publicación Técnica*, *5*, 40.

Cisternas, A., & Vera, E. (2008). Sismos históricos y recientes en Magallanes. *Magallania (Punta Arenas)*, *36*, 43–51.

Connon, G. C., Bollini, M. C., Sabbione, N. C., & Hormaechea, J. L. (2021). Complemento 2017–2020 del Catálogo Sismológico de Referencia de Tierra del Fuego.

Cunningham, W. D. (1993). Strike-slip faults in the southernmost Andes and the development of the Patagonian orocline. *Tectonics*, *12*, 169–186.

Cunningham, W. D. (1995). Orogenesis at the southern tip of the Americas: The structural evolution of the cordillera Darwin metamorphic complex, southernmost Chile. *Tectonophysics*, *244*, 197–229.

Dalziel, I. W., & Brown, R. L. (1989). Tectonic denudation of the Darwin metamorphic core complex in the Andes of Tierra del Fuego, southernmost Chile: Implications for cordilleran orogenesis. *Geology*, *17*(8), 699–703.

Dalziel, I. W., Lawver, L. A., Norton, I. O., & Gahagan, L. M. (2013). The scotia arc: Genesis, evolution, global significance. *Annual Review of Earth and Planetary Sciences*, *41*, 767–793.

De Batist, M., Talling, P., Strasser, M., & Girardclos, S. (2017). Subaquatic paleoseismology: Records of large Holocene earthquakes in marine and lacustrine sediments. *Marine Geology*, *384*, 1–3.

de La Taille, C., Jouanne, F., Crouzet, C., Beck, C., Jomard, H., de Rycker, K., & Van Daele, M. (2015). Impact of active faulting on the post LGM infill of Le Bourget Lake (western Alps, France). *Tectonophysics*, *664*, 31–49.

Delvaux, D., & Sperner, B. (2003). Stress tensor inversion from fault kinematic indicators and focal mechanism data: The TENSOR program. In: New insights into structural interpretation and modelling (D. Nieuwland ed.). *Geological Society, London, Special Publications*, *212*, 75–100.

Doughty, M., Eyles, N., & Eyles, C. (2013). High-resolution seismic reflection profiling of neotectonic faults in Lake Timiskaming, Timiskaming graben, Ontario-Quebec, Canada. *Sedimentology*, *60*, 983–1006.

Esteban, F., Bran, D. M., Tassone, A., Menichetti, M., Lodolo, E., Lippai, H., & Vilas, J. F. (2013). The structures of the Peninsula Ushuaia in the Beagle Channel (Tierra del Fuego, Argentina). *Rendiconti Online Societa Geologica Italiana*, *29*, 43–46.

Febrer, J. M., Plasencia, M. P., & Sabbione, N. C. (2000). Local and regional seismicity from Ushuaia broadband station observations (Tierra del Fuego). *Terra Antartica*, *8*, 35–40.

Forsyth, D. W. (1975). Fault plane solutions and tectonics of the South Atlantic and Scotia Sea. *Journal of Geophysical Research*, *80*, 1429–1443.

Ghiglione, M. C., Yagupsky, D., Ghidella, M., & Ramos, V. A. (2008). Continental stretching preceding the opening of the Drake Passage: Evidence from Tierra del Fuego. *Geology*, *36*, 643–646.

Gordillo, S., Bujalesky, G. G., Pirazzoli, P. A., Rabassa, J. O., & Saliège, J.-F. (1992). Holocene raised beaches along the northern coast of the Beagle Channel, Tierra del Fuego, Argentina. *Palaeogeography, Palaeoclimatology, Palaeoecology*, *99*, 41–54.

Hall, B. L., Porter, C. T., Denton, G. H., Lowell, T. V., & Bromley, G. R. (2013). Extensive recession of cordillera Darwin glaciers in southernmost South America during Heinrich stadial 1. *Quaternary Science Reviews*, *62*, 49–55.

Jaschek, E. U., Sabbione, N. C., & Sierra, P. J. (1982). *Reubicación de sismos localizados en territorio Argentino, 1920–1963*. Observatorio Astronomico de la Universidad nacional de la Plata.

Klepeis, K., Betka, P., Clarke, G., Fanning, M., Hervé, F., Rojas, L., Mpodozis, C., & Thomson, S. (2010). Continental underthrusting and obduction during the Cretaceous closure of the Rocas Verdes rift basin, Cordillera Darwin, Patagonian Andes. *Tectonics*, *29*(3), TC3014.

Klepeis, K. A. (1994). The Magallanes and Deseado fault zones: Major segments of the south American-Scotia transform plate boundary in southernmost South America, Tierra del Fuego. *Journal of Geophysical Research: Solid Earth*, *99*, 22001–22014.

Lagabrielle, Y., Suárez, M., Rossello, E. A., Hérail, G., Martinod, J., Régnier, M., & de la Cruz, R. (2004). Neogene to quaternary tectonic evolution of the Patagonian Andes at the latitude of the Chile triple junction. *Tectonophysics*, *385*, 211–241.

Livermore, R., Hillenbrand, C.-D., Meredith, M., & Eagles, G. (2007). Drake Passage and Cenozoic climate: An open and shut case? *Geochemistry, Geophysics, Geosystems*, *8*(1), Q01005.

Livermore, R., Nankivell, A., Eagles, G., & Morris, P. (2005). Paleogene opening of Drake passage. *Earth and Planetary Science Letters*, *236*, 459–470.

Lodolo, E., Donda, F., & Tassone, A. (2006). Western Scotia Sea margins: Improved constraints on the opening of the Drake Passage. *Journal of Geophysical Research: Solid Earth*, *111*(B6), B06101.

Lodolo, E., Menichetti, M., Bartole, R., Ben-Avraham, Z., Tassone, A., & Lippai, H. (2003). Magallanes-Fagnano continental transform fault (Tierra del Fuego, southernmost South America). *Tectonics*, *22*(6), 1–17.

Lodolo, E., Menichetti, M., Guzmán-Speziale, M., Giunta, G., & Zanolla, C. (2009). Deep structural setting of the North American-Caribbean plate boundary in eastern Guatemala. *Geofisica Internacional*, *48*(3), 263–277.

Maldonado, A., Bohoyo, F., Galindo-Zaldívar, J., Hernández-Molina, F. J., Lobo, F. J., Lodolo, E., Martos, Y. M., Pérez, L. F., Schreider, A. A., & Somoza, L. (2014). A model of oceanic development by ridge jumping: Opening of the Scotia Sea. *Global and Planetary Change*, *123*, 152–173.

McCalpin, J. P. (2009). *Paleoseismology*. Academic press.

McCulloch, R. D., Blaikie, J., Jacob, B., Mansilla, C. A., Morello, F., De Pol-Holz, R., San Román, M., Tisdall, E., & Torres, J. (2020). Late glacial and Holocene climate variability, southernmost Patagonia. *Quaternary Science Reviews*, *229*, 106131.

McCulloch, R. D., Mansilla, C. A., Morello, F., De Pol-Holz, R., San Roman, M., Tisdall, E., & Torres, J. (2019). Late glacial and Holocene

landscape change and rapid climate and coastal impacts in the canal beagle, southernmost Patagonia. *Journal of Quaternary Science, 34,* 674–684.

Mendoza, L., Perdomo, R., Hormaechea, J. L., Del Cogliano, D., Fritsche, M., Richter, A., & Dietrich, R. (2011). Present-day crustal deformation along the Magallanes–Fagnano fault system in Tierra del Fuego from repeated GPS observations. *Geophysical Journal International, 184,* 1009–1022.

Mendoza, L., Richter, A., Fritsche, M., Hormaechea, J. L., Perdomo, R., & Dietrich, R. (2015). Block modeling of crustal deformation in Tierra del Fuego from GNSS velocities. *Tectonophysics, 651,* 58–65.

Menichetti, M., Lodolo, E., & Tassone, A. (2008). Structural geology of the Fuegian Andes and Magallanes fold-and-thrust belt-Tierra del Fuego Island. *Geologica Acta, 6,* 19–42.

Minster, J. B., & Jordan, T. H. (1978). Present-day plate motions. *Journal of Geophysical Research: Solid Earth, 83,* 5331–5354.

Mörner, N. A. (1991). Holocene Sea level changes in the Tierra del Fuego region. *Boletim IG-USP. Publicação Especial, 8,* 133–151.

Nelson, E. P., Dalziel, I. W. D., & Milnes, A. G. (1980). Structural geology of the cordillera Darwin–collision style orogenesis in the southernmost Andes. *Eclogae Geologicae Helveticae, 73,* 727–751.

Obrist-Farner, J., Eckert, A., Locmelis, M., Crowley, J. L., Mota-Vidaure, B., Lodolo, E., Rosenfeld, J., & Duarte, E. (2020). The role of the Polochic fault as part of the north American and Caribbean plate boundary: Insights from the infill of the Lake Izabal Basin. *Basin Research, 32*(6), 1347–1364.

Onorato, M. R., Perucca, L. P., Coronato, A., Prezzi, C., Blanc, P. A., López, R., & Magneres, I. (2021). Morphotectonic characterization along the eastern portion of the main trace of Magallanes-Fagnano fault system in Tierra del Fuego, Argentina. *Journal of South American Earth Sciences, 112,* 103550.

Onorato, M. R., Perucca, L. P., Coronato, A. M. J., López, R., & Blanc, P. (2020). Evidencias morfotectónicas en el sistema de fallas Magallanes–Fagnano, borde transformante entre las placas Sudamericana y Scotia, Isla Grande de Tierra del Fuego, Argentina. *Revista de la Asociación Geológica Argentina, 77,* 47–61.

Pelayo, A. M., & Wiens, D. A. (1989). Seismotectonics and relative plate motions in the Scotia Sea region. *Journal of Geophysical Research: Solid Earth, 94,* 7293–7320.

Peroni, J. I., Tassone, A., Menichetti, M., & Cerredo, M. E. (2009). Geophysical modeling and structure of Ushuaia pluton. *Fuegian Andes, Argentina, Tectonophysics, 476,* 436–449.

Rabassa, J., Coronato, A., Bujalesky, G., Salemme, M., Roig, C., Meglioli, A., Heusser, C., Gordillo, S., Roig, F., & Borromei, A. (2000). Quaternary of Tierra del Fuego, southernmost South America: An updated review. *Quaternary International, 68,* 217–240.

Rabassa, J., Coronato, A., Roig, C., Martínez, O., Serrat, D., Blanco, R., López, J., Pérez Alberti, A., 2004. Un bosque sumergido en Bahía Sloggett, Tierra del Fuego, Argentina: evidencia de actividad neotectónica diferencial en el Holoceno tardío. *Procesos geomorfológicos y evolución costera-2 Reunión Geomorfología Litoral,* Santiago de Compostela, Spain. 333–345.

Rabassa, J., Heusser, C., & Stuckenrath, R. (1986). New data on Holocene sea transgression in the Beagle Channel: Tierra del Fuego, Argentina. *International Symposium on Sea-Level Changes and Quaternary Shorelines, 1,* 291–309.

Roy, S., Vassallo, R., Martinod, J., Ghiglione, M. C., Sue, C., & Allemand, P. (2020). Co-seismic deformation and post-glacial slip rate along the Magallanes-Fagnano fault, Tierra Del Fuego, Argentina. *Terra Nova, 32,* 1–10.

Sabbione, N., Connon, G., Hormaechea, J., & Rosa, M. (2007). Estudio de sismicidad en la provincia de Tierra del Fuego, Argentina. *Geoacta, 32,* 41–50.

Sandoval, F. B., & De Pascale, G. P. (2020). Slip rates along the narrow Magallanes fault system, Tierra Del Fuego region, Patagonia. *Scientific Reports, 10,* 1–13.

Sue, C., & Ghiglione, M. C. (2016). Wrenching tectonism in the southernmost Andes and the Scotia Sea constrained from fault kinematic and seismotectonic overviews. In *Geodynamic evolution of the southernmost Andes* (pp. 137–171). Springer.

Vérard, C., Flores, K., & Stampfli, G. (2012). Geodynamic reconstructions of the South America–Antarctica plate system. *Journal of Geodynamics, 53,* 43–60.

Villalobos, A., Easton, G., Maksymowicz, A., Ruiz, S., Lastras, G., De Pascale, G. P., & Agurto-Detzel, H. (2020). Active faulting, submarine surface rupture, and seismic migration along the Liquiñe-Ofqui fault system, Patagonian Andes. *Journal of geophysical research: Solid Earth, 125,* e2020JB019946.

Waldmann, N., Anselmetti, F. S., Ariztegui, D., Austin, J. A., Jr., Pirouz, M., Moy, C. M., & Dunbar, R. (2011). Holocene mass-wasting events in Lago Fagnano, Tierra del Fuego (54°S): Implications for paleoseismicity of the Magallanes-Fagnano transform fault: Holocene mass-wasting events in Lago Fagnano, Tierra del Fuego (54°S). *Basin Research, 23,* 171–190.

Zanolla, C., Lodolo, E., Lippai, H., Tassone, A., Menichetti, M., Baradello, L., Grossi, M., & Hormaechea, H. L. (2011). Bathymetric map of Lago Fagnano (Tierra del Fuego Island). *Bollettino di Geofisica Teorica Ed Applicata, 52,* 1–8.